Vortex structures in $YBa_2Cu_3O_7$ (invited)

B. Keimer
Department of Physics and Princeton Materials Institute, Princeton University, Princeton, New Jersey 08544 and National Institute of Standards and Technology, Gaithersburg, Maryland 20899

J. W. Lynn and R. W. Erwin
National Institute of Standards and Technology, Gaithersburg, Maryland 20899

F. Dogan
Princeton Materials Institute and Department of Chemical Engineering, Princeton University, Princeton, New Jersey 08544

W. Y. Shih
Princeton Materials Institute, Princeton University, Princeton, New Jersey 08544

I. A. Aksay
Princeton Materials Institute and Department of Chemical Engineering, Princeton University, Princeton, New Jersey 08544

Extensive small angle neutron scattering experiments have been conducted on the vortex system in $YBa_2Cu_3O_7$ in a magnetic field range of $0.5\ T \leq H \leq 5\ T$, and with various orientations of the magnetic field with respect to the crystallographic axes. For H parallel to the c axis, the vortex lattice is oblique with two nearly equal lattice constants and an angle of 73° between primitive vectors. One principal axis of the vortex lattice coincides with the (110) direction of the crystal lattice. It is shown that this structure cannot be explained in the framework of a purely electrodynamic (London) model, and that it is intimately related to the in-plane anisotropy of the superconducting coherence length. When the field is inclined with respect to the c axis, the uniaxial anisotropy due to the layered crystal structure of $YBa_2Cu_3O_7$ becomes relevant. The interplay between the square in-plane anisotropy and the uniaxial anisotropy leads to both a continous structural transition and a reorientation of the vortex lattice as a function of inclination angle. For the largest inclination angles, the vortex lattice decomposes into independent chains.

I. INTRODUCTION

The vortex system in the cuprate superconductors has received a high level of attention mostly because of its novel phase behavior inferred from transport experiments at high temperatures and high magnetic fields. Small angle neutron scattering (SANS) is applicable in high magnetic fields and capable of measuring the relevant correlation lenghts of the vortex lattice. SANS is therefore very promising as a tool to further elucidate this behavior. However, since the signal intensity at high temperatures is very small, these experiments are difficult. Our approach has therefore been to first develop a thorough experimental description of the vortex system at low temperatures as a function of field strength and field orientation with respect to the crystallographic axes, before studying thermal effects in detail. We have found that the behavior of the vortex lattice is very rich even at low temperatures. In particular, our experiments indicate a close relation between the structure of the vortex lattice and the microscopic electronic structure of $YBa_2Cu_3O_7$. The following is a preliminary summary of these studies.

II. EXPERIMENTAL DETAILS

Our sample is a disk-shaped single crystal of $YBa_2Cu_3O_7$ of volume $\sim 2.5\ cm^3$ and mosaicity $\sim 1.5°$. The sample is too large to fit into a superconducting quantum interference device (SQUID) magnetometer, but small pieces cut off from samples prepared under identical conditions showed sharp superconducting transitions at ~93 K. The microstructure of these samples has been extensively characterized by transmission electron microscopy. Prominent microstructural features are μm sized Y_2BaCuO_5 inclusions with a total volume fraction ~10%, twin boundaries of average separation ~900 Å extending in the (110) or $(1\bar{1}0)$ crystallographic directions, and stacking faults perpendicular to the (001) direction. The latter two features occur on length scales comparable to intervortex distances and therefore give rise to background small angle scattering in the experimentally relevant range of scattering angles. This (temperature independent) background is comparable to or larger than the magnetic scattering from the vortex lattice and must be subtracted from the raw data.

All experiments were performed on the NG-3 and NG-7 SANS spectrometers at the Cold Neutron Research Facility of the National Institute of Standards and Technology. We mostly used the standard horizontal-field scattering geometry[1] with the neutron beam almost parallel to the magnetic field. Horizontal magnetic fields of 0.5 T or less were generated by an electromagnet, larger fields were achieved in a horizontal-field superconducting magnet. For some experiments we also used a vertical-field electromagnet.

The experimental geometry is illustrated in Fig. 1. The x (horizontal) axis in this figure is the magnetic field direction. The scattered neutrons are collected as a function of the coordinates y and z perpendicular to the field by an area detector behind the sample. During the experiment the angle be-

 0021-8979/94/76(10)/6778/6/$6.00

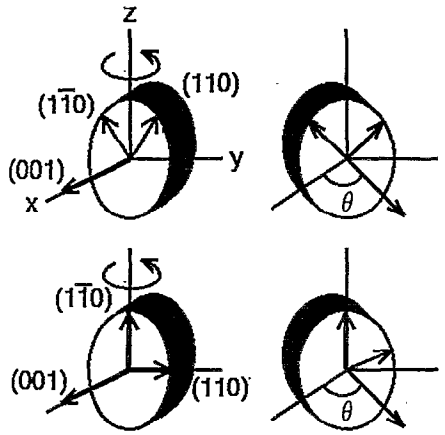

FIG. 1. Coordinate system illustrating the experimental geometry of our experiments. The x axis is the magnetic field direction. The neutron beam is almost parallel to the magnetic field (i.e., the scattering angle is small). The angle θ (rotation angle around $\hat{z}$ relative to the x axis) can be changed during the experiment. The orientation of the crystalline axes with respect to x,y,z is chosen by orienting the crystal outside the cryostat. Two different crystal orientations are shown: (top) (100) parallel to $\hat{z}$ and (bottom) (110) parallel to $\hat{z}$. The axes $\hat{y}$ and $\hat{z}$ perpendicular to the magnetic field are the horizontal and vertical axes in the diffraction patterns below.

tween the neutron beam and the magnetic field (i.e., the scattering angle ϑ) can be varied, and the sample can be turned around the vertical $\hat{z}$ axis without remounting the sample. We denote the angle between the crystalline (001) direction and the magnetic field by θ. The crystallographic direction coinciding with the $\hat{z}$ axis is selected by orienting the sample by x-ray and thermal neutron scattering outside the cryostat. We chose three different sample orientations: (i) (100) parallel to $\hat{z}$ (Fig. 1, top); (ii) (110) parallel to $\hat{z}$ (Fig. 1, bottom); and (iii) a low-symmetry crystallographic direction parallel to $\hat{z}$ (not shown). A uniform flux profile within the sample is achieved by field cooling the crystal for each crystal orientation. Typical counting times for high quality diffraction patterns are several hours.

In order to optimize both resolution and signal intensity, different spectrometer settings were chosen at each magnetic field. We mostly used neutrons of wavelengths 5 or 6 Å and wavelength spread $\Delta\lambda/\lambda=0.31$, source and sample apertures of 5 and 1.27 cm diameter, respectively, and source-to-sample distances between 11 and 13 m. A parameter of particular importance is the angular resolution in the plane of the area detector (yz plane in Fig. 1). At a given wavelength and source aperture (chosen to optimize the neutron flux on the sample), this quantity is primarily controlled by the distance between the sample and the detector.[2] For larger magnetic fields (corresponding to larger scattering angles), smaller sample-to-detector distances can be chosen, and the angular resolution is improved. On the other hand, because of the decreasing form factor the signal-to-background ratio becomes worse for larger fields. We found that data of optimal overall quality could be taken for $H=2$ T.

III. VORTEX LATTICE SYMMETRY AND ELECTRONIC STRUCTURE

Early SANS experiments on $YBa_2Cu_3O_7$ for $H=0.8$ T revealed a diffraction pattern with fourfold symmetry when

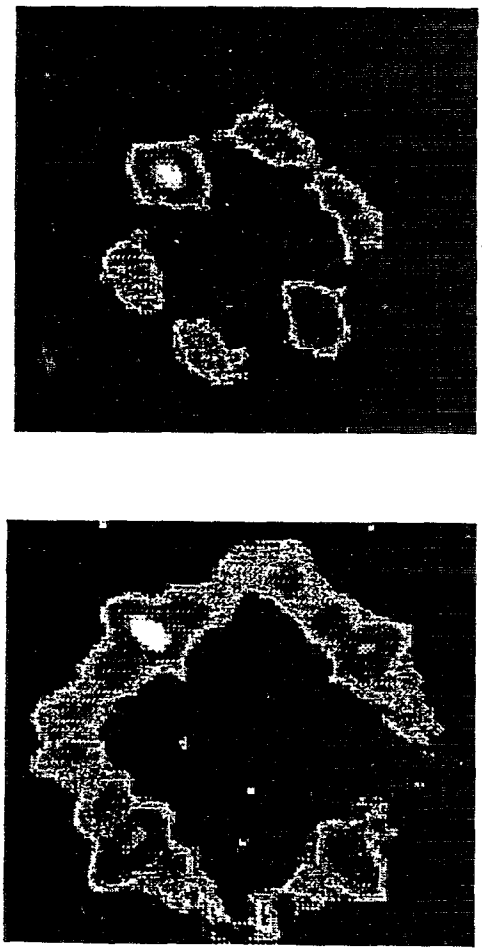

FIG. 2. Grey scale images of SANS diffraction patterns taken for (top) $H=0.5$ T, $\theta\sim10°$, obtained by rotating around a low-symmetry crystallographic direction and (bottom) $H=2$ T, $\theta=0$.

the magnetic field is aligned with the (001) crystalline direction.[3] This pattern was subsequently shown to consist of two sixfold symmetric patterns with 90° relative orientation.[4] However, the angular resolution of these patterns was not sufficient to determine the structure of the vortex lattice for this field orientation in detail. We have now used the improved angular resolution achievable in higher magnetic fields to resolve this issue definitively. The bottom panel of Fig. 2 shows that a total of 16 weak and 4 strong Bragg reflections can be resolved for fields of 2 T and above. (Note that all patterns shown here are for ϑ fixed. Since by Bragg's law each reflection corresponds to a different ϑ, not all of the 20 spots appear in a single pattern. The remaining spots can be moved into the resolution volume by adjusting ϑ appropriately.)

The real-space lattice corresponding to this diffraction pattern, shown in Fig. 3, can be regarded as intermediate between triangular (with an angle of $\beta=60°$ between primitive vectors) and square (corresponding to $\beta=90°$). In a high resolution measurement at $H=2$ T we obtained $\beta=(73\pm1)°$. We also found that the lattice constants differ by $(5\pm5)\%$; the unit cell area satisfies the flux quantization rule within the experimental accuracy. We can therefore not distinguish

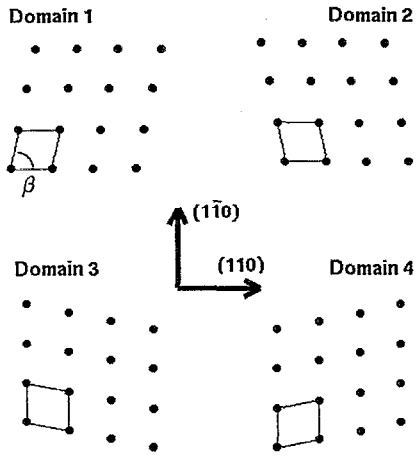

FIG. 3. Real-space structures corresponding to the diffraction patterns of Fig. 2. The top pattern of that figure is taken under conditions in which only two of the domains are populated (1 and 2, or 3 and 4). In the bottom pattern all four domains are populated.

experimentally between oblique (unequal lattice constants, space group $p2$) or rectangular (equal lattice constants, space group $c2mm$) vortex lattice symmetry. As the figure indicates, four domains with different orientations of the unit cell are observed. One of the nearest-neighbor directions of the vortex lattice coincides with either the (110) or the (1$\bar{1}$0) direction of the crystal lattice. Superposition of the diffraction patterns of these four domains results in the experimentally observed pattern of Fig. 2; the four strong reflections originate from two domains, the 16 weak reflections from one domain. A deconvolution of the patterns for $H=0.5$ T and $H=5$ T which takes the appropriate spectrometer resolution into account yields the same value for β. Note that with the spectrometer settings that had to be chosen for $H=0.5$ T two of the weak spots could not be resolved completely (Fig. 2, top).

When H is precisely aligned with the c axis, these four domains are degenerate and occupy equal fractions of the sample volume. However, the degeneracy between the domains is lifted even by a subtle inclination of the field with respect to the c axis. Tilting often favors two of the domains over the remaining two, as shown in Fig. 2. The mechanism for creation of this domain imbalance will be discussed in the next section.

The oblique structure we observe is manifestly different from the triangular lattice expected when the vortices interact purely electrodynamically. We have therefore evaluated the Gibbs free energies of vortex lattices with different β, taking the nonzero extent of the vortex core into account. In the London approximation, the Gibbs free energy density can be written as[5]

$$G=\frac{B^2}{8\pi}\left(\sum_{Q}\frac{1}{1+\lambda^2Q^2}\right)-\frac{HB}{4\pi}, \tag{1}$$

where $\lambda\sim1500$ Å is the penetration depth, B is the magnetic induction, and the sum runs over all reciprocal lattice vectors Q. The finite extent of the vortex core is approximated by a circular "hard core" cutoff $Q_{\max}=2\pi/\xi$, where $\xi\sim15$ Å is the in-plane coherence length. At each applied field H and for each β the magnetic induction, B, is computed by numerically evaluating $\partial G/\partial B=0$. While at low magnetic fields our calculation is insensitive to the size of the vortex core and reproduces the well-known free energy minimum at $\beta=60°$, $G(\beta)$ becomes extremely sensitive to the core cutoff in fields of several tesla. Typical numerical data are shown in Fig. 4. This means that the structure of the vortex core begins to have a significant influence on the structure of the vortex lattice in the field regime investigated in our experiments. The shape of the vortex core and the behavior of the superconducting order parameter near the core reflect the underly-

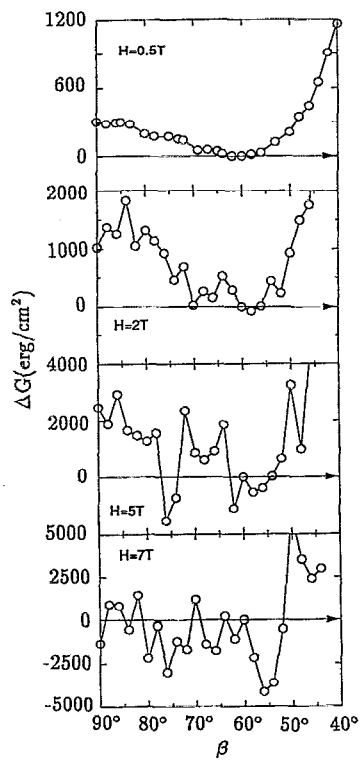

FIG. 4. Numerically computed Gibbs free energy density of a vortex lattice with space group $c2mm$ and angle β between primitive vectors (Fig. 3), relative to the triangular lattice ($\beta=60°$). The calculations are based on Eq. (1) with $\lambda=1500$ Å and $\xi=16$ Å. The numerical errors are much smaller than the symbol size.

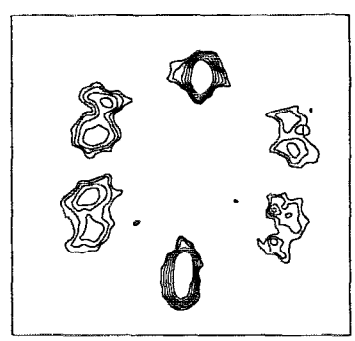

FIG. 5. Contour plot of SANS pattern for $H=2$ T, $\theta=20°$, obtained by rotating around (110).

ing microscopic electronic structure of the superconductor, in particular the spatial variation of the energy gap.

The link between the microscopic electronic structure and the mesoscopic structure of the vortex lattice is provided by the gap equation in a magnetic field. Even for an isotropic Bardeen–Cooper–Schrieffer (BCS) superconductor this equation is difficult to solve at a general magnetic field. Additional difficulties arise in the cuprates because the functional form of the gap equation is still under debate. However, as first shown by Abrikosov,[6] the equations simplify significantly near the upper critical field, where the magnetic induction is almost uniform. While for isotropic superconductors the equilibrium vortex lattice structure is the triangular lattice near H_{c2},[7] a $c2mm$ structure of the type we observe here has been observed before in the cubic superconductor Nb,[8] when the field is oriented in a fourfold crystallographic direction. This observation was explained theoretically by Takanaka,[9] who solved the gap equation of a superconductor with a cubic Fermi surface and found that in general structures of $c2mm$ symmetry have lower free energies than the triangular lattice. The angle β between primitive vectors depends on the degree of Fermi surface anisotropy through the parameter $\langle e^{i4\varphi}\rangle$, where φ is the azimuthal angle in the yz plane perpendicular to the magnetic field, and the brackets denote an average on the Fermi surface. We have parametrized the Fermi surface extracted from photoemission experiments[10] by two harmonics invariant under the point symmetry of the lattice

$$E_F(\varphi)=E_{F0}+E_{F1}\sin^2\varphi\cos^2\varphi, \tag{2}$$

with $E_{F1}\approx E_{F2}$, and obtain $\langle e^{i4\varphi}\rangle\approx E_{F1}/16E_{F0}$. According to the numerical calculations of Ref. 9, this value of $\langle e^{i4\varphi}\rangle$ corresponds to $\beta=63°$, much closer to 60° than the angle we observe. The origin of this discrepancy is likely to be an energy gap anisotropy contributed by the pairing interaction in the cuprates. It is already known that significant modifications to the standard gap equation are needed to account for the large directional variation of the energy gap observed in photoemission experiments on $Bi_2Sr_2CaCu_2O_{8+\delta}$.[11] Another possible origin of the quantitative discrepancy between theory and our observations is an in-plane penetration depth anisotropy, which various authors have determined to be between ~1.1 (Ref. 12) and ~1.5.[13] While a quantitative explanation of our data thus has to await more elaborate calculations based on realistic gap equations, it is remarkable that the symmetry of the vortex lattice is correctly predicted by an analysis whose only ingredient is the fourfold symmetry of the vortex core.

A more extensive treatment of anisotropic vortex lattices in type-II superconductors with a small ratio of penetration depth to coherence length has been given by Teichler,[14] who considered a cubic superconductor with an anisotropic pairing interaction. The resulting gap anisotropy leads to an attractive interaction between the vortices, in addition to the electrodynamic repulsion. The magnitude of the attractive interaction is largest in the direction of minimum energy gap, which is the (110) direction in $Bi_2Sr_2CaCu_2O_{8+\delta}$(Ref. 11) and presumably also in $YBa_2Cu_3O_7$. Teichler's analysis will likely need substantial modifications in the case of $YBa_2Cu_3O_7$. In particular, the energy gap in the (110) direction is extremely small and possibly zero, which may lead to a long range interaction between vortices. Nevertheless, the directional variation of the energy gap in the CuO_2 planes is a plausible explanation for the observed coupling between vortex lattice and crystal lattice orientations.

We[4] and others[3] had previously attributed this unique orientation of the vortex lattice to pinning by twin boundaries. However, the persistence of this orientation even as the field is inclined by up to 40° with respect to the twin boundaries is difficult to reconcile with this model. Moreover, the persistence of the same structure over an order of magnitude in magnetic field which we have now observed argues against a significant influence of twin boundaries on the vortex lattice structure and orientation. (Whereas at $H=0.5$ T the intervortex distance is comparable to the average twin boundary spacing, at $H=5$ T it is almost five times smaller.)

Since near H_{c1} the size of the vortex core is negligible compared to the intervortex distance, vortex core effects cannot play a role in determining the vortex lattice structure and orientation in very low magnetic fields. Indeed, Bitter decoration experiments near H_{c1} have revealed the expected triangular lattice with an orientation unrelated to any crystalline high-symmetry direction.[12,15] We thus expect a crossover between an orientationally degenerate triangular lattice and the oblique structure with unique orientation in an intermediate field range. There are some indications that this crossover actually occurs at a very low field, as expected for a large gap anisotropy: For $B\sim0.0065$ T, close to the largest field for which the Bitter decoration technique is applicable, Dolan *et al.*[13] observed a structure that is completely consistent with the one we observed (Fig. 3), except that $\beta=(65°\pm5°)$. Note that these measurements were taken in untwinned sections of $YBa_2Cu_3O_7$ crystals, further supporting our argument for an intrinsic origin of the coupling between the crystal lattice and vortex lattice. The field independence of β in the field range we have investigated suggests that β has already saturated at its H_{c2} value.

IV. TILT-INDUCED STRUCTURAL TRANSITION

We observe a potentially related structural transition as the magnetic field is inclined by an angle θ with respect to the c axis. This transition is superposed by an overall distortion of the vortex lattice due to the quasi two dimensionality of the electronic structure.[4,16] For inclination angles up to $\theta\sim60°$, the structure of the vortex lattice remains dominated by interactions within the CuO_2 sheets. The vortex lattice for small θ can thus be thought of as the projection of an isotropic two-dimensional lattice onto the field direction. This effect gives rise to an elliptical distortion of the vortex lattice; the semimajor axis of the ellipse coincides with $\hat{H}\times\hat{c}$, and the aspect ratio is $\cos\theta$ for small θ. (As three-dimensional interactions become relevant for larger θ, the aspect ratio becomes $\sqrt{\epsilon^2\sin^2\theta+\cos^2\theta}$, where $\epsilon\sim0.2$ is the penetration depth anisotropy.)

In addition to this overall anisotropy, we observe a continuous structural transition of the in-plane isotropic lattice as a function of θ: The angle $\beta=73°$ observed for $\theta\sim0$ de-

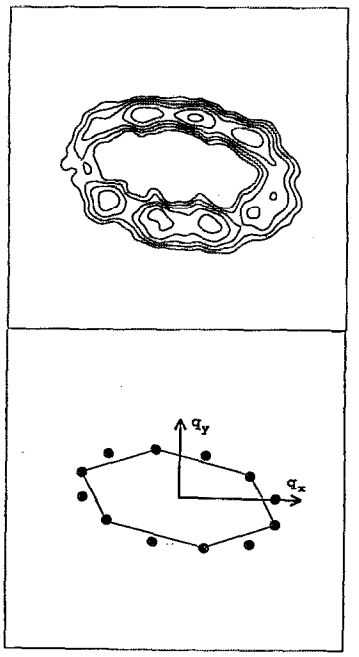

FIG. 6. (Top) contour plot of SANS pattern for $H=0.5$ T, $\theta=60°$, obtained by rotating around a low-symmetry crystallographic direction. (Bottom) projection of two isotropic triangular lattices in the CuO_2 layers onto the field direction for the same geometry. The lattices are oriented such that nearest-neighbor pairs point in either the (110) or the $(1\bar{1}0)$ direction. One of these domains is highlighted.

creases continuously and reaches $\beta=60°$, corresponding to the triangular lattice, for $\theta\sim50°$ (Fig. 6). The nearest-neighbor direction remains the in-plane (110) direction.

While the structural transition occurs for all three experimental geometries discussed in Sec. I, the domain structure of the observed lattice depends on the crystallographic direction chosen as the axis of rotation. If the field inclination is achieved by rotating around (100), all four domains of Fig. 3 continue to be populated. However, once β has reached 60°, domains 1 and 2, as well as domains 3 and 4, become identical. If the rotation axis is (110), a two-domain lattice is observed (Fig. 5). For the two observed domains, the projection of $(1\bar{1}0)$ is parallel to the direction $\hat{H}\times(\hat{H}\times\hat{c})$, i.e., the y axis in Fig. 1. [Note that the diffraction pattern can be obtained from the real lattice by a 90° rotation and rescaling, and that because of twinning (110) and $(1\bar{1}0)$ are superposed in our crystal.] This is the nearest-neighbor direction favored by the uniaxial anisotropy reflecting the quasi two-dimensional electronic structure.[17] The uniaxial anisotropy can thus lift the degeneracy between the domains.

We have also chosen an experimental geometry in which the inclination is achieved by rotating around a low-symmetry crystallographic direction such that (110) and $(1\bar{1}0)$ subtend identical angles with the rotation axis.[4] In this case we also observe a two-domain lattice for small θ, although the uniaxial anisotropy does not distinguish between the two domain pairs. However, the vortices in the two domain pairs subtend different angles with respect to both sets of twin boundaries.[4] Pinning interactions between vortices and twin boundaries favor the pair of domains subtending the smaller angle with respect to the twin boundaries, because the vortices have to bend less in order to gain advantage of the pinning energy. Although, as discussed above, the structure and orientation of the vortex lattice are determined by electronic energies that are presumably much larger than pinning energies, pinning effects appear to provide enough energy to select between otherwise degenerate domains.

It may not be coincidental that the triangular structure observed in inclined fields is just the structure expected in the London limit, since the in-plane vortex lattice is only sensitive to a reduced field component $H\cos\theta$ perpendicular to the CuO_2 sheets. Moreover, for large θ the effective core size shrinks because of the reduced coherence length in the c-axis direction. Electrodynamic effects should thus become more relevant for larger inclinations. Detailed numerical calculations to test these ideas are currently underway.

V. TILT-INDUCED REORIENTATION AND VORTEX CHAIN STATE

In agreement with this general scenario, we observe a reorientation of the vortex lattice into the unique orientation predicted by the anisotropic London model when the inclination is achieved by rotating around (100). In this case the orientation favored by the in-plane energy gap anisotropy is different from the orientation favored by the anisotropic electrodynamic interactions between the vortices. For small θ the electrodynamic energies favoring the $\hat{H}\times(\hat{H}\times\hat{c})$ direction as the nearest-neighbor direction are small,[17] and the in-plane anisotropy determines the vortex lattice orientation. As the shielding currents around the vortices begin to flow in the c-axis direction for large θ, in-plane anisotropy effects diminish and the electrodynamic effects associated with the uniaxial penetration depth anisotropy begin to dominate. The crossover between these two orientations is gradual and begins at $\theta\sim70°$ in this geometry, coming to completion for $\theta\sim80°$.

In the large-θ orientation, the vortex lattice can be considered as a collection of chains with locked periodicity extending in the $\hat{H}\times(\hat{H}\times\hat{c})$ direction. Because of the penetration depth anisotropy, the distance between the chains is much larger than the nearest-neighbor distance within the chains. Based on calculations in the London limit, an extremely small modulus for shear in the chain direction has been predicted,[18] thus causing a decoupling of the chains even for very weak pinning disorder or thermal fluctuations. This vortex chain state has indeed been observed in Bitter decoration experiments in very low magnetic fields.[19] We have observed the same instability in fields of 0.5 and 2 T. Its experimental signature is a continuous broadening of all Bragg reflections not exclusively associated with the distance between the chains. For $\theta=80°$ only the two reflections with Bragg planes parallel to the chain direction remain sharp and observable. Note that all of our diffraction patterns were taken after field cooling the sample to low temperatures. The disordered vortex chain state is thus presumably frozen in at high temperatures.

We have carefully measured the width of the "rocking curves" of the vortex chain state reflections at $H=0.3$ T, using a vertical-field electromagnet. This measurement pro-

vides direct information about the "straightness" of the vortices in the bulk of the sample. A temperature dependence of the rocking curve could thus herald dimensional crossover effects or thermal wandering of three-dimensional vortices. We find that the rocking curves, as well as the width of the reflections perpendicular to the field direction, remain resolution limited up to at least $T=80$ K. The signal-to-background ratio became too low to extract reliable information from measurements taken at higher temperatures. We plan to repeat these measurements in higher magnetic fields, where we expect the conditions to be more favorable.

VI. CONCLUSIONS

In conclusion, we have demonstrated an unanticipated connection between the vortex lattice structure in magnetic fields of order 1 T and the microscopic electronic structure of $YBa_2Cu_3O_7$. As a result of the directional variation of the energy gap in the CuO_2 plane, the symmetry and orientation of the vortex lattice is coupled to the underlying crystal lattice when the field is applied in the c-axis direction. This coupling diminishes gradually as the field is inclined with respect to the c axis. As a function of increasing inclination angle we observe a two-step transition of the vortex lattice into the symmetry and orientation predicted by the London model with uniaxial anisotropy.

ACKNOWLEDGMENTS

We are grateful to C. Glinka and J. Rush for their support and advice, and to V. J. Emery, H. F. Hess, D. E. Moncton, N. P. Ong, and M. Yethiraj for helpful discussions. This work is based upon activities supported by the National Science Foundation under Agreement No. DMR-9122444. The work at Princeton was supported by the Advanced Research Projects Agency and the Air Force Office of Scientific Research under Grants AFOSR No. F49620-90-C-0079 and No. F49620-93-I-0259.

[1] G. Lippmann, J. Schelten, and W. Schmatz, Philos. Mag. **33**, 475 (1976).
[2] J. S. Pedersen, D. Posselt, and K. Mortensen, J. Appl. Crystallogr. **23**, 321 (1990).
[3] E. M. Forgan *et al.*, Physica C **185–189**, 247 (1991); M. Yethiraj *et al.*, Phys. Rev. Lett. **70**, 857 (1993).
[4] B. Keimer *et al.*, Science **262**, 83 (1993)
[5] M. Tinkham, *Introduction to Superconductivity* (Krieger, Malabar, 1975).
[6] A. A. Abrikosov, Zh. Exp. Teor. Fiz. **32**, 1442 (1957); Sov. Phys. JETP **5**, 1174 (1957).
[7] W. H. Kleiner, L. M. Roth, and S. H. Autler, Phys. Rev. **133**, A1226 (1964).
[8] J. Schelten, G. Lippmann, and H. Ullmaier, J. Low Temp. Phys. **14**, 213 (1974).
[9] K. Takanaka, Prog. Theor. Phys. **46**, 1301 (1971); **49**, 64 (1973).
[10] J. C. Campuzano *et al.*, Phys. Rev. Lett. **64**, 2308 (1990).
[11] Z.-X. Shen *et al.*, Phys. Rev. Lett. **70**, 1553 (1993).
[12] G. J. Dolan *et al.*, Phys. Rev. Lett. **62**, 2184 (1989).
[13] K. Zhang and D. A. Bonn *et al.*, preprint.
[14] H. Teichler, Philos. Mag. **30**, 1209 (1974); **31**, 789 (1975); K. Fischer and H. Teichler, Phys. Lett. A **58**, 402 (1976).
[15] P. L. Gammel, in *Phenomenology and Applications of High-Temperature Superconductors* (Addison–Wesley, New York, 1992).
[16] M. Yethiraj *et al.*, Phys. Rev. Lett. **71**, 3019 (1993).
[17] L. J. Campbell, M. M. Doria, and V. G. Kogan, Phys. Rev. B **38**, 2439 (1988); L. J. Campbell and V. G. Kogan, Phys. Rev. Lett. **62**, 1552 (1989).
[18] B. I. Ivlev and N. B. Kopnin, Phys. Rev. B **44**, 2747 (1991); B. I. Ivlev, N. B. Kopnin, and M. M. Salomaa, *ibid.* **43**, 2896 (1991).
[19] P. L. Gammel *et al.*, Phys. Rev. Lett. **68**, 3343 (1992).